Available online at www.sciencedirect.com
SCIENCE DIRECT®
International Journal of Heat and Mass Transfer 47 (2004) 5703–5712
International Journal of HEAT and MASS TRANSFER
www.elsevier.com/locate/ijhmt

Spray cooling characteristics of water and R-134a. Part I: nucleate boiling

Shou-Shing Hsieh *, Tsung-Cheng Fan, Huang-Hsui Tsai

Department of Mechanical and Electro-Mechanical Engineering, National Sun Yat-Sen University, Kaohsiung 80424, Taiwan, ROC

Received 1 December 2003; received in revised form 16 June 2004
Available online 17 September 2004

Abstract

An experimental study was made in the first of two papers to determine the effect of liquid sprays used to cool a hot surface. Both pure water and R-134a were served as a working medium sprayed from a single circular nozzle onto a Cu (oxygen free) metal of an electrically heated surface which was heated to an initial temperature with a range of wall superheat for steady-state nucleate boiling experiments using thermocouples for heat transfer measurements. Cooling characteristics (boiling curves) were obtained over a range of spray mass flux, Weber number, wall superheat and degree of subcooling. Boiling visualization was also conducted with varied heat flux levels at a specified *We* for R-134a and water.

1. Introduction

Spray cooling with phase change has been received much attention and industrial applications such as emergency cooling, microelectronics cooling, and fire extinguishment due to its extremely high heat removed capability within a considerable short time and at low wall superheat. The importance of these applications has motivated research into understanding of the mechanism of heat removal by sprays with plenty of literatures published; however, there seems quite a few papers dealing with the spray cooling topics by using refrigerants as a working medium especially for non-CFC refrigerants and their associated applications in refrigeration and air conditioning industry. In addition, a detailed surface temperature measurement using the transient liquid crystal(TLC) technique seems to have not been explored yet for spray cooling.

It is long recognized [1] that spray cooling with phase change has been demonstrated to be a powerful method to remove high heat flux (>1000 W/cm^2) from surfaces with a considerable low wall superheat. Choi and Yao [2] experimentally studied the effect of heater orientation through droplet impingements. It was found that a higher heat transfer happened in film boiling for a vertical spray jet; while for a horizontal spray jet, a higher heat transfer occurred in transition boiling. Gonzalez and Black [3] reported a finding that the interaction between spray and buoyant jet issued from a heated surface would reduce the droplet velocity. Most recently, Yoshida et al. [4] experimentally investigated the effect of microgravity for spray cooling using water and FC-72 as the working medium. It was found that the gravity dependency of the spray cooling characteristics varies with the spray volume flux and the droplet Weber number.

* Corresponding author. Tel.: +886 7 5252000x4215; fax: +886 7 5254215.
E-mail address: sshsieh@mail.nsysu.edu.tw (S.-S. Hsieh).

0017-9310/$ - see front matter © 2004 Elsevier Ltd. All rights reserved.
doi:10.1016/j.ijheatmasstransfer.2004.07.022

Nomenclature

A	area of test surface, m^2
Bo_m	modified boiling number, $qx/\mu h_{fg}$
C_p	specific heat for spray liquid, kJ/kg °C
d	droplet mass median diameter, μm
d_j	nozzle diameter, m
d_{32}	Sauter mean diameter (SMD), μm
g	gravitational acceleration, m/s^2
h	heat transfer coefficient, W/m^2 °C
h_{fg}	enthalpy of evaporation, kJ/kg
Ja	Jacob number, $(c_l\Delta T)/h_{fg}$
m	spray mass flux, $kg/m^2 s$
P_{sat}	saturation pressure, MPa
ΔP	pressure difference, MPa
q	heat flux, W/m^2
q_{CHF}	critical heat flux, W/m^2
T_l	liquid temperature, °C
T_w	wall temperature, °C
T_{sat}	saturation temperature, °C
u_j	spray velocity at the nozzle exit, m/s
u_0	mean spray impingement velocity, m/s
We	spray Weber number, $\rho_l u_0^2 d_{32}/\sigma$
x	distance from nozzle to test surface, m

Greek symbols

α	spray cone angle
ΔT	$T_w - T_l$, °C
ΔT_{sat}	wall superheat, °C
ΔT_{sub}	degree of subcooling, °C
ρ	density of liquid, kg/m^3
σ	surface tension of spray liquid, N/m

There are two different physical phenomena for spray cooling. One is steady-state boiling in which three distinct regions exist [1]; namely, forced convection and evaporation, nucleate boiling region, and critical heat flux. The other is transient cooling in which film boiling and transition boiling play an important role [4]. It will be discussed in detail in the second paper (Part II). Generally speaking, the droplets sprayed onto the heated surface will form flat disks of which its thickness is much lower than the diameter of the droplet. Meanwhile, the stagnation flow field spreads the droplets and disk further to form a thin liquid film on the surface through shear forces. In fact, boiling in droplets deposited on a hot surface differs from that observed in a pool boiling, since heat transfer relies on the contact area between the droplets and surface [5].

Based on the aforementioned discussion, most previous findings seem concentrated on the influence of gravity and the thickness of a liquid film on the heater surface [1] on spray cooling characteristics. Only a few papers mentioned using CFC refrigerants liquid spray [6,7]; moreover, for non-CFC refrigerants, such information and document are even more inadequate. In fact, substantial differences in heat transfer with phase change were observed [4] between water and organic liquids. It is essentially necessary to complement the existing data by providing the related information and document for non-CFC refrigerants at this stage.

This work presents the results of liquid sprays of both pure water and R-134a. The variation of surface temperature was measured during cooling. The spray mass flux, the Weber number, and wall superheat as well as the liquid degree of subcooling on spray characteristics were extensively examined. Moreover, spray impact as well as detailed heat transfer coefficient distribution by using TLC technique was photographed (Part II). Key objectives of this study (Part I) are to

1. develop a better understanding of how working fluid and spray mass flux influence the cooling performance,
2. visualize the spray boiling phenomena,
3. generalize a heat flux correlation which can be applied to water and R-134a with Weber number and relevant parameters.

2. Experimental

2.1. General

Fig. 1 is a schematics of the apparatus used for spray cooling experiments. It consists of a nozzle-spray system, test surface, and a temperature measurement system, which were housed in a stainless steel cylindrical chamber (250 mm long × 200 mm dia.) with a glass sheet top ceiling. A circular sight glass was made in front of the chamber with a dimension of ID 140 mm, and centered at the 100 mm below the top of the test chamber.

In the nozzle-spray system, a commercially available full-cone ($\alpha = 80°$) spray circular nozzle with a diameter $d_j = 0.38$ mm (M1, Sprayer Co. Ltd) was used to achieve different values (6.4×10^{-2}–3.06×10^{-1} $kg/m^2 s$) of liquid mass flux sprayed onto the test surface. The spray nozzle located normal to and directly above the center of the upward-facing test surface. The nozzle provided presumably uniform coverage with wall temperature differences less than 2 °C over the test surface. The droplet size and

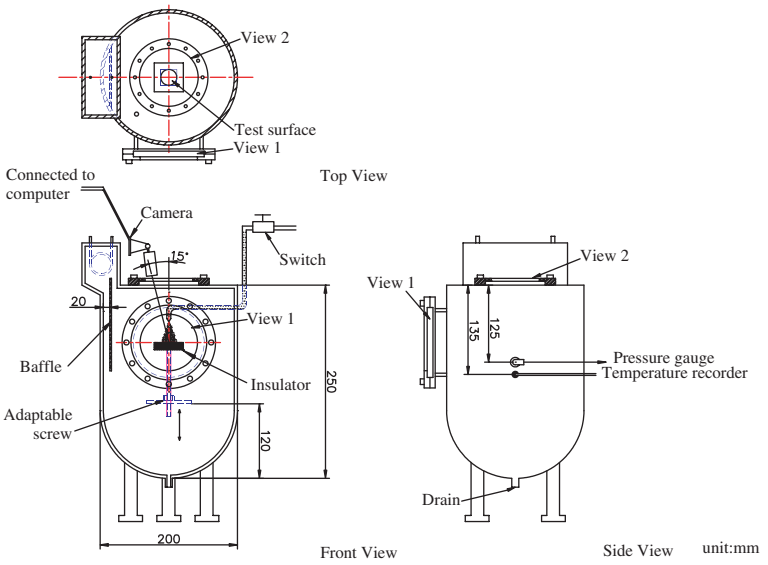

Fig. 1. Experimental test facility.

velocity distribution depend on the liquid flow rate and were provided by the nozzle supplier.

A copper block heater was prepared for use in two different experiments, steady-state (Part I) and transient experiment (Part II), respectively. Fig. 2 illustrates the structure of a cylinder copper disk heater with an oxygen free Cu metal electroplated circular surface of 8 mm diameter with a 75 μm thickness (Part I)/or a Pt-sputtered surface of the same diameter with 0.5 μm thickness (Part II) on its flat end and completely covered by the spray cone in either case. Regarding the heater surface characteristics, the heater is designed to allow a low thermal capacity mass with a relative large test surface to reach a rapid and fine control while the spray cooling is occurring. The test surface was placed at a distance $x = 60$ mm (this distance is fixed for the present study) from the nozzle tip, centered along the axis of the spray. Four 0.3 mm diameter chromel–alumel (K type) thermocouples were inserted into holes drilled with 90° interval apart and 15 mm depth, positioned 0.075 mm (Cu) and 0.005 mm (Pt) below the test surface, respectively. The holes were filled with a high

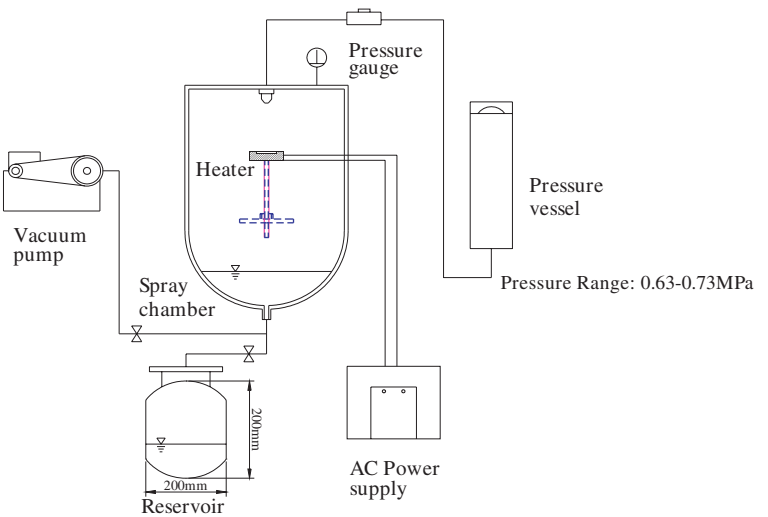

Fig. 2. Experimental test loop.

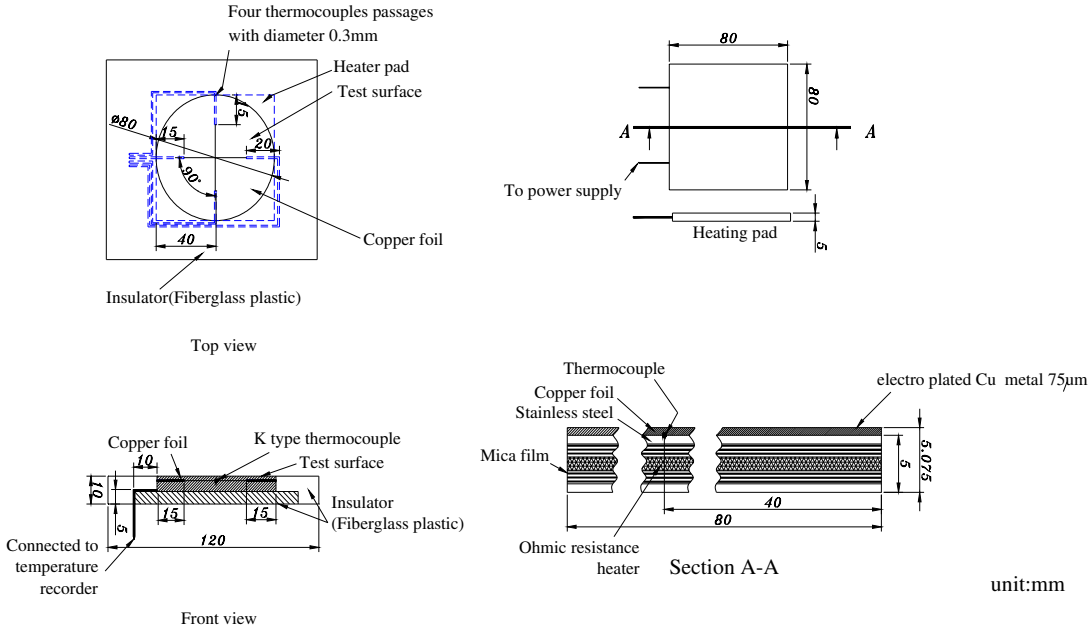

Fig. 3. Heater and thermocouple configuration.

thermal conductivity spray cement (alumina/silica; $k = 8.4\,\mathrm{W/m\,°C}$) to minimize the thermal contact resistance before inserting four thermocouples. In addition, to obtain a detailed heat transfer data, the TLC technique was also applied (will be discussed in Part II). The test chamber was insulated to reduce heat losses. The heater surface was of square geometry with a side length of 80 mm (Fig. 3).

The local heat flux q were obtained from $q = q_{in} - q_c - q_r$ where q_{in} is heat input equal to VI and q_c and q_r are heat losses due to conduction and radiation. In fact, q_r is quite small wrt the other terms and considered to be negligible. Corrections to surface temperatures were made via one dimensional heat conduction equation. The uniformity of the surface temperature distribution indicated that the uniformity cooling of the surface existed. The maximum difference in wall temperature did not exceed 2 °C. An arithmetic average of the wall temperature was used for heat transfer calculations.

Spray cooling tests were performed using both pure (distilled) water and R-134a refrigerant, for steady-state experiments (Part I). The disk was gradually heated to higher temperatures (<100 °C for both fluids) before the CHF conditions were reached. Simultaneously, the change in heat flux with test surface temperature was continuously monitored and recorded. Before the experiments, the test surface was cleaned first with metal polish, then washed with acetone, and finally exposed to distilled water.

2.2. Spray parameters

The mean velocity of spray droplets impinged on the test surface was estimated by the following equation [8]

$$u_0 = \left(u_j^2 + \frac{2\Delta P}{\rho} - \frac{12\sigma}{\rho d} - 2gx\right)^{0.5} \tag{1}$$

For the present study, the first term of the RHS of Eq. (1) dominates; i.e., neglecting the remaining three contributions (<1%). Three nozzle pressures were used in the present study for each fluid as shown in Table 1. Noting that d in Eq. (1) is the mean median droplet diameter obtained from the following equation,

$$d = 9.5 d_j \Big/ \left(\Delta P^{0.37} \sin\frac{\alpha}{2}\right) \tag{2}$$

where ΔP, d_j and α (=80°) represent the pressure drop between the nozzle pressure and test chamber pressure, the nozzle diameter, and the nozzle spray angle.

The spray mass flux at test surface was calculated for different pressure drop by replacing the test surface with a section of copper tubing with the same internal diameter as the surface area as well as with the tubing exit pressure identical to the chamber pressure, and recording the volume of liquid flowing into the tubing within a known time period. The measurements above were estimated to be accurate within ±6%.

The Sauter mean diameter (SMD), d_{32}, was used to calculate the spray Weber number. It was provided by

Table 1
The geometric of test section and dynamic parameters

The diameter of test section (mm)	80					
Test surface to nozzle distance, H (mm)	60					
Nozzle diameter, D (mm)	0.38					
Working medium	R-134a			Water		
Nozzle pressure (MPa)	0.62	0.67	0.72	0.15	0.20	0.25
Mass flow rate, m (kg/s)	4.52×10^{-4}	6.06×10^{-4}	7.6×10^{-4}	1.24×10^{-3}	1.68×10^{-3}	2.13×10^{-3}
Spray mass flux, m (kg/m^{2}s)	0.064	0.086	0.108	0.178	0.24	0.306
Droplet diameter (jet exit), d (μm)	79	68	61	79	68	61
Impact velocity (at the center of test surface), u_0 (m/s)	2.85	4.04	5.19	10.34	14.38	23.29
Mean spray impact diameter, d_{32} (μm)	46	44	42	46	44	42
Weber number, We	50	96	152	80	148	231
Jet Reynolds number, Re_j	165	221	277	220	295	370
Power supply	0–600 W					
Degree of subcooling (°C)	2–4			55–60		

the nozzle supplier and the Weber number was defined, $\rho_l u_0^2 d_{32}/\sigma$.

The spray parameters mentioned above with other operating variables are summarized in Table 1.

2.3. Boiling visualization

Photographs of spray droplets impinged on the test surface were taken using a Panasonic 26×87 mm CCD camera with a speed of 3 frames/s. Illumination was provided by a cool white fluorescent lamp which is the same as for the TLC measurement (Part II). Photographs were taken using an Eastman Kodak TMAX 400 film and exposure times ranging from 1/50 to 1/1000 s with an aperture of f 2.0. Meanwhile, a video camera (Sony DCR-TRV 800) was simultaneously used to record the images of spray impingement on the test surface. The video signal was fed to a personal computer through a

Table 2
Uncertainties of relevant parameters/variables

Parameters/variables	Uncertainties		
Radius of test surface, r		±0.625%	
Heat surface area, A		±0.884%	
Saturation temperature, T_{sat}	R-134a	16 °C	±0.315%
		18 °C	±0.278%
	Water	80 °C	±0.06%
		85 °C	±0.058%
Wall temperature, T_w	⊙		±0.062%
	⊕		±0.23%
ΔT	⊙		±0.118%
	⊕		±0.605%
Electric current, I	⊙		±7.1%
	⊕		±0.68%
Voltage, V	⊙		±5.6%
	⊕		±0.51%
Total heat transfer rate, Q	⊙		±9.04%
	⊕		±1.05%
Heat flux, q	⊙		±9.06%
	⊕		±1.05%
Heat transfer coefficient, h	⊙		±9.1%
	⊕		±1.29%

Note: ⊕ max. heat input 160,000 W/m^2, ⊙ min. heat input 2000 W/m^2.

RGB decoder and a data translation frame grabber. The computer controlled the selection of sequences of up to 500 frames with an area of 128×162 pixels to be recorded from each frame.

3. Uncertainty analysis

An uncertainty analysis was made to consider the errors caused by the interpolation procedure of the measuring instruments. The uncertainty is due to calibration and fluctuation in the thermocouple reading during spray cooling. The values of the four wall temperatures were recorded and compared to examine variations caused either by non-uniformities in the heating pad or by the test surface bonding and assembly procedure. The uncertainty in various primary variables is summarized in Table 2 at minimum/maximum heat input, respectively.

4. Results and discussion

4.1. Cooling performance/boiling curves (steady-state nucleate boiling)

R-134a at 14 °C was sprayed onto the heater surface at varying operating pressure and flow rates. The heat flux and wall temperature were determined simultaneously as the wall surface was gradually heated. Fig. 4 shows the heat transfer characteristics for three different spray mass flux in terms of Weber number. There seems to be two or three distinct regions existing in the curves shown in Fig. 4 as also reported by Yang et al. [1]. In the first region, forced convection and evaporation are the modes of heat transfer. As the heat flux is increased gradually, the slope at the curve changed where nucleate boiling begins. Due to the greater magnitude of the latent heat as compared to the sensible heat for forced convection, the heat transfer increases steeply. The third region may occur at $We = 152$. At this stage, according to Yang et al. [1], no liquid reaches the edge of the test surface other than through the direct spray. The Weber number effect is clearly noted. The number characterizes the impacting dynamics of the droplet. The cooling performance increased as *We* increased because the high *We* impeded the fraction of a vapor blanket between the test surface and the droplet.

The effect of subcooling seems not significant as shown in Fig. 4. It is perhaps because the subcooling of R-134a were only 2 and 4 °C, respectively. In fact, it has been found in traditional nucleate boiling experiments that the cooling performance would decrease with subcooling [9]. However, this situation would change a bit. It appears that sprays will theoretically diminish less because the impacting dynamics are thought to improve

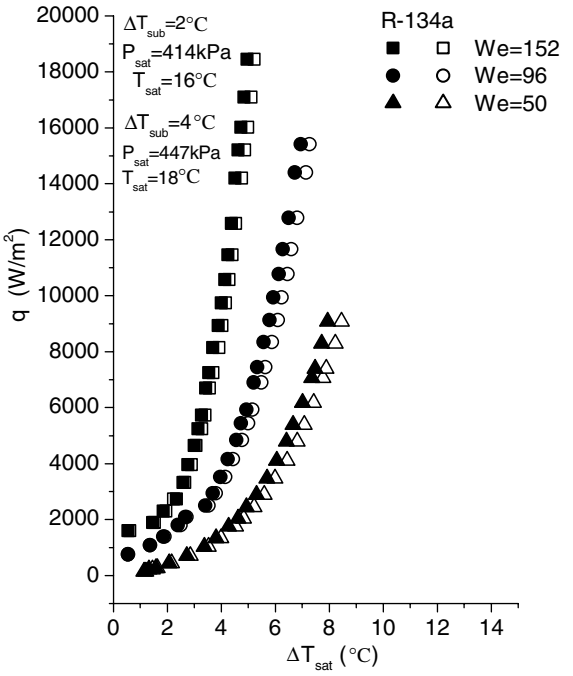

Fig. 4. Steady-state nucleate boiling curve (solid symbols: $\Delta T_{sub} = 2$ °C, open symbols: $\Delta T_{sub} = 4$ °C).

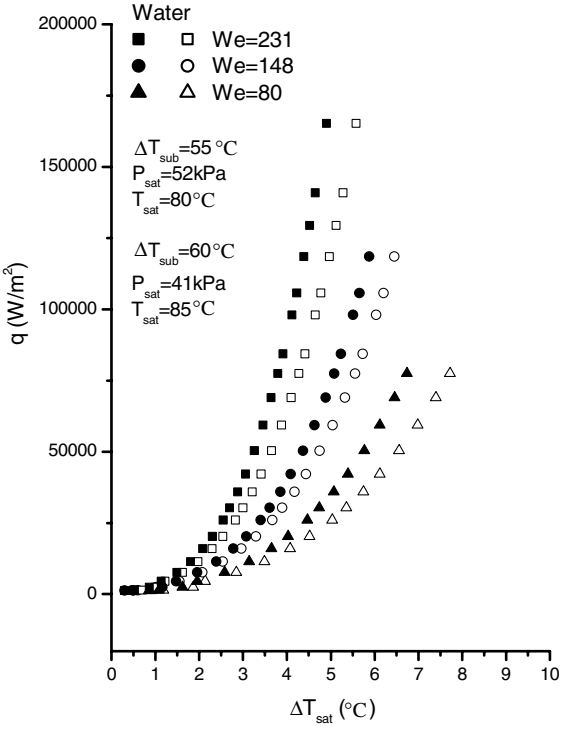

Fig. 5. Steady-state nucleate boiling curve (solid symbols: $\Delta T_{sub} = 55$ °C, open symbols: $\Delta T_{sub} = 60$ °C).

resistance of vapor nuclei to subcooling and have been proven to have a lower nucleation superheat once saturation conditions have been restored. This can be seen in Fig. 4 if not considering experimental uncertainty that the cooling performance with $\Delta T_{sub} = 2\,^{\circ}C$ is little bit better than that with $\Delta T_{sub} = 4\,^{\circ}C$. In addition, the evaporation process inside the liquid spray will be isolated from the subcooled bulk liquid.

By contrast, pure water at 25 °C was sprayed onto the heater surface, with two different subcoolings ($\Delta T_{sub} = 55\,^{\circ}C$ and $60\,^{\circ}C$), and three different spray mass flux as listed in Table 1. The results were shown in Fig. 5. Again, Weber number effect is clearly seen. In addition, degree of subcooling on cooling performance can be also clearly noted in water. Both fluids (R-134a and water) show that the onset of nucleation is about 2–4 °C with a decrease in *We*. The subcooling effect shown in Fig. 5 is significant as compared to that for R-134a shown in Fig. 4. Also, this effect becomes important for both fluids as *We* decreases. Both figures (Figs. 4 and 5) can also be found from the transient cooling curves experiments in Part II of this paper.

The Weber number effect is displayed in the *h–q* curves shown in Figs. 6 and 7, respectively, for R-134a and water. Noting that the *h* here indicates an average heat transfer coefficient. The average heat transfer coefficient h increases as the heat flux increases in the power (exponent) of nearly 0.595 ± 0.013. Detailed data for the correlation for each case were tabulated in Table 3. This value was little bit higher than that of Yoshida et al. [4] for water and a little lower than most impingement boiling heat transfer studies, e.g. Zhou and Ma [10] for R-113 within acceptable range. Generally, water has a heat transfer superior to R-134a and *h* is about $6.0 \times 10^3\,W/m^2\,^{\circ}C$ at $q = 2 \times 10^4\,W/m^2$ and at $We = 148$, for example (Fig. 7). On the other hand, in Fig. 6, the corresponding

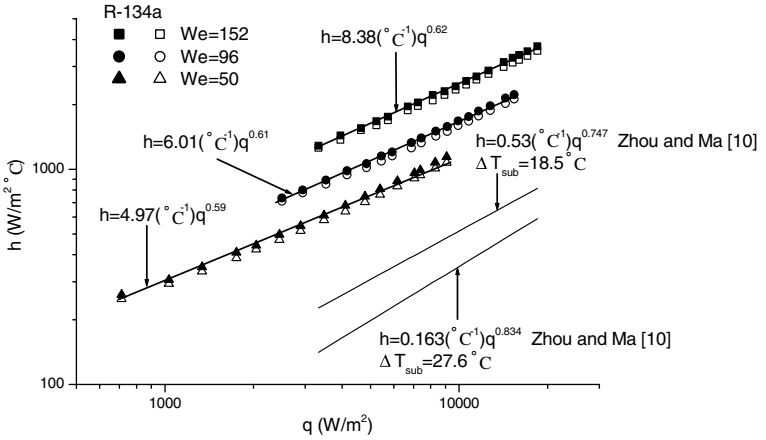

Fig. 6. *h–q* curves (solid symbols: $\Delta T_{sub} = 2\,^{\circ}C$, open symbols: $\Delta T_{sub} = 4\,^{\circ}C$).

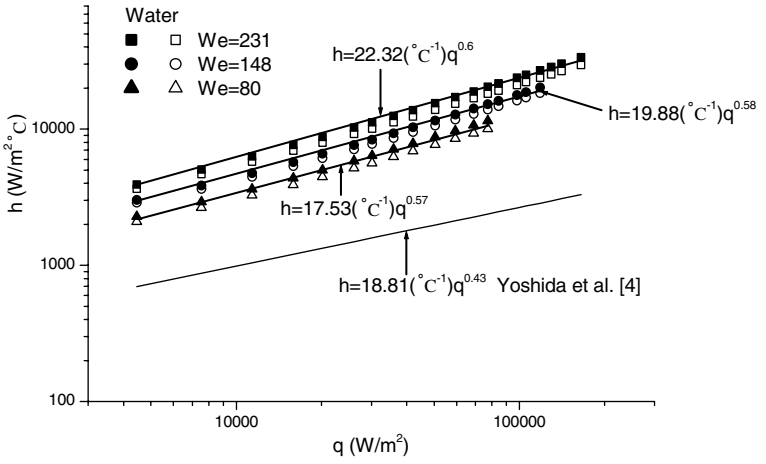

Fig. 7. *h–q* curves (solid symbols: $\Delta T_{sub} = 55\,^{\circ}C$, open symbols: $\Delta T_{sub} = 60\,^{\circ}C$).

Table 3
Correlations of nucleate boiling curves for water and R-134a

Fluids	ΔT_{sub} (°C)	*We*	$h = C_1 q^m$	
			C_1 (°C^{-1})	*m*
R-134a	2	50	4.97	0.59
		96	6.01	0.61
		152	8.38	0.62
	4	50	4.97	0.59
		96	6.01	0.61
		152	8.38	0.62
Water	55	80	17.53	0.57
		148	19.88	0.58
		231	22.32	0.6
	60	80	17.53	0.57
		148	19.88	0.58
		231	22.32	0.6

(at the same q and *We*) h is about 4.0×10^3 W/m^2 °C for R-134a with different degree of subcoolings. In general, in the spray cooling process, the liquid droplets can penetrate the vapor blanket as compared to pool nucleate boiling to maintain contact between the thin liquid and the heated surface so that a higher heat transfer coefficient can be obtained (Figs. 6 and 7). In fact, if compared with those in saturation pool boiling, the present spray cooling heat transfer coefficient is about 200% higher than its counterpart [11] for R-134a. This difference is mainly caused by the mechanisms of spray cooling that enhance heat transport through phase change [1].

4.2. Boiling visualization

Fig. 8 shows typical top views of the test surfaces at three different heat flux levels for R-134a and water at a specified Weber number, respectively. Generally, the dark portions indicate that there are liquid films; while for bright portions, indicate the dry areas of the test surface. Noting that photographs taken were made an angle of 15° with vertical axis. This resulted in the present photographs looking like an elliptic shape rather than a circle. Based on these two sets of photographs, it was found again that the droplet impact behavior in this nucleate boiling regime looks similar for all three *We*. The flow boiling involved in the present spray cooling process can be explained generally as follows: it was found that the bubbles first appeared on the edge of the test surface because as the liquid film flows from the center of the test surface toward the edge of the surface, the liquid film continuously absorbed heat through forced convection or nucleate boiling, which results in the saturation conditions being reached first on the edge of the surface at a low Weber number (e.g. $We \leqslant 50$ (R-134a)/or $\leqslant 80$(water)). After the liquid droplets extend themselves completely, the liquid reshaped under the action of surface tension into a globule (an island) which was rebounded off the test surface. In the middle Weber number range, $50(80) \leqslant We \leqslant 96(148)$ for R-134a(water), similar phenomena were found for $We < 50(80)$ except that, upon deforming and rebounding, the droplet would split into a number of globules (islands) and spherical droplets. As the Weber number

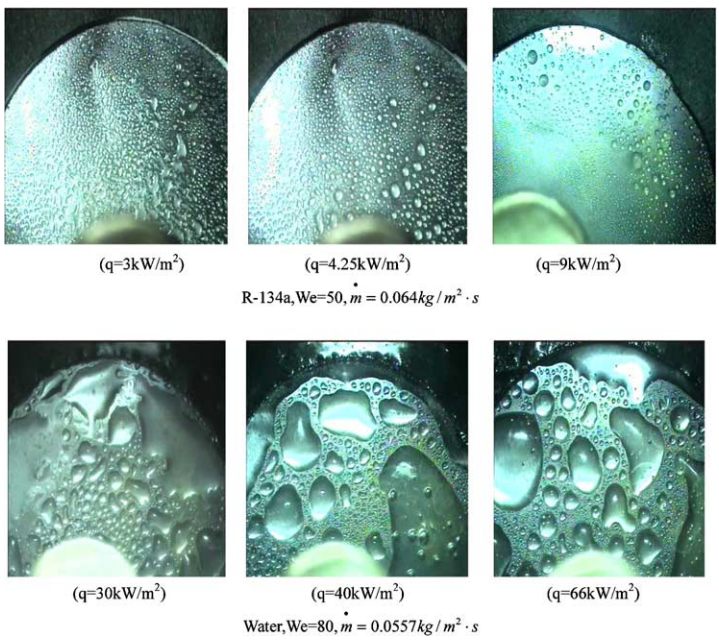

Fig. 8. Observation of R-134a and water sprayed on heater surface.

is even higher, $We > 96(148)$, the droplets start to spread out radially into a flat disk which broke up violently into plenty of small droplets.

Following the discussion above, the photographs shown in Fig. 8 can be illustrated in sequence. When the spray mass flux was low (i.e., low *We*), it was observed that the liquid droplet formed a number of small liquid films showing an island-like (globule-like as stated above) behavior, which partially covered the test surface and, at the same time, the droplets impinging on the rest dry area immediately evaporated. As the Weber number increases, plenty of globules and small spherical droplets would be formed due to droplets deformation and rebound. Relevant discussion of the associated droplet impact dynamics will be found in Part II of this paper. Overall, the present boiling visualization is consistent with the TLC detailed heat transfer distribution measurements in Part II of this paper.

4.3. Correlation for the relevant parameters (*We*, *Ja*, Bo_m)

Following Ghodbane and Holman [6], a correlation with a series variables/parameters of q, ΔT, *We* and μ_l was developed with a specified x to examine its applicability (for R-134a and water) and generality where x stands for the distance between the nozzle exit and test surface which is fixed in the present study.

It was found that a general correlation, similar to that given by Ghodbane and Holman [6], was again found with almost the same exponents appearing in *We* and *Ja* term. However, different constant coefficient multipliers resulted. As a result, the spray cooling heat flux (in terms of modified Boiling number, Bo_m) with subcooled R-134a and water is correlated in the form of

$$Bo_m = C(We)^m(Ja)^n \tag{3}$$

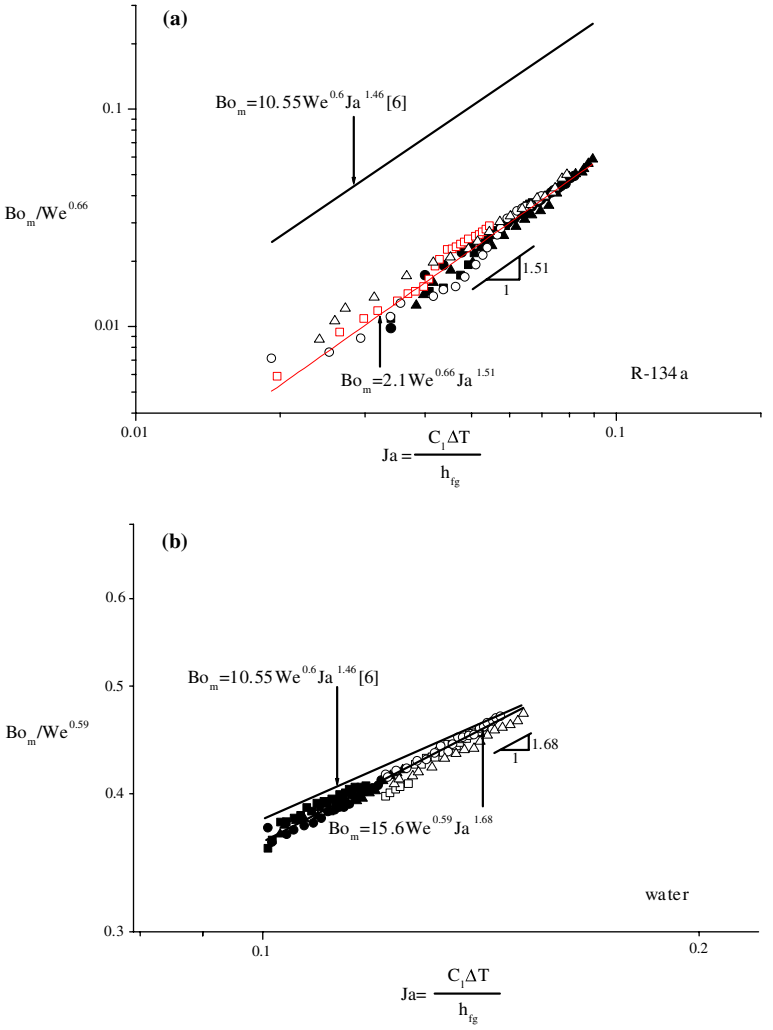

Fig. 9. Correlation of R-134a and water.

where $Ja = C_l\Delta T/h_{fg}$ is Jacob number, this number takes into account both convective and boiling heat transfer effect, and $Bo_m = qx/\mu_l h_{fg}$ stands for modified boiling number. This Bo_m using a length scale of x rather than a conventional bubble diameter. This correlation was plotted in Figs. 9(a) and (b), for R-134a and water, respectively. Also included in Figs. 9(a) and (b) is the R-113 results from [6] for comparison. Noting that the present correlation is suitable for both forced convection and nucleate boiling (i.e., for spray cooling). It was found that the coefficients C and powers of m and n of Eq. (3) were 2.1, 0.66, and 1.51 for R-134a and 15.6, 0.59, and 1.68 for water, respectively. The heat transfer is strongly dependent on We and Ja as the power values of m and n show in Figs. 9(a) and (b). Based on the magnitude of C for R-134a and water, it is obvious that the heat transfer performance of water is much better than that of R-134a approximately (15.7 vs 2.1) due to the water having a much higher latent heat. However, the value of the coefficient C for present R-134a results is about five times smaller than the value of 10.55 used by Ghodbane and Holman [6]. The major reason for this difference is mainly due to the much higher spray mass flux of R-113 and different thermophysical properties of the fluid used in Ghodbane and Holman [6]. Furthermore, in fact, the present study is for a vertical impinged spray; however, the report from Ghodbane and Holman [6] is a horizontal spray. This may also indicate that the effect of test surface orientation on spray cooling performance is significant. The above explanations may also be assessed by the results of water, which seem to have the equal magnitude of Bo_m shown in Fig. 9(b). Actually, the present water results were found to be 1.5–2 times higher than those of R-134a as stated previously. Consequently, this results in an nearly same Bo_m due to a much higher latent heat of water as compared to organic fluids like R-134a and R-113 as indicated in Fig. 9(b).

5. Conclusion

A series of experiments were conducted on the effect of different working media, degree of subcoolings, and spray mass fluxes used for cooling of a hot surface. Spray mass flux in terms of We has a strong effect on spray cooling performance. However, the effect of degree of subcooling is not clearly noted especially for R-134a due to a low degree of subcooling used. Even though, a delayed onset of saturated boiling was found for water with high degree of subcoolings (55 and 60 °C). Water shows a much higher spray cooling performance than that of R-134a. Finally, a correlation was developed of which it has the form of $Bo_m = C(We)^m(Ja)^n$ with nearly the same m and n and different C for both fluids as one would expect.

References

[1] J. Yang, L.C. Chow, M.R. Pais, Nucleate boiling heat transfer in spray cooling, ASME J. Heat Transfer 118 (1996) 668–671.
[2] K.J. Choi, S.C. Yao, Mechanism of film boiling heat transfer of normally impacting spray, Int. J. Heat Transfer 30 (1987) 311–318.
[3] J.E. Gonzalez, W.Z. Black, Study of droplet sprays prior to impact on a heater horizontal surface, ASME J. Heat Transfer 119 (1997) 279–287.
[4] K. Yoshida, Y. Abe, T. Oka, Y.H. Mori, A. Nagashima, Spray cooling under reduced gravity condition, ASME J. Heat Transfer 123 (2001) 309–318.
[5] Q. Cui, S. Chandra, S. MeCahan, The effect of dissolving salts in water spray used for quenching a hot surface. Part 1: boiling of single droplets, ASME J. Heat Transfer 125 (2003) 326–332.
[6] M. Ghodbane, J.P. Holman, Experimental study of spray cooling with freon-113, Int. J. Heat Mass Transfer 34 (1991) 1163–1174.
[7] M. Kato, Y. Abe, Y.H. Mori, A. Nagashima, On the spray cooling characteristics under reduced gravity, AIAA J. Thermophys. Heat Transfer 9 (1995) 378–381.
[8] Y.M. Qiao, S. Chandra, Spray cooling enhancement by addition of a surfactant, ASME J. Heat Transfer 120 (1998) 92–98.
[9] S.S. Hsieh, K.-J. Jang, M.-T. Huang, Evaporative heat transfer and enhancement performance of serpentine tubes with strip-type inserts using refrigerant-134a, ASME J. Heat Transfer 121 (1999) 752–757.
[10] D.W. Zhou, C.F. Ma, Local jet impingement boiling heat transfer with R-113, Heat Mass Transfer 40 (2003) 88–99.
[11] S.S. Hsieh, C.C. Weng, J.J. Chiou, Nucleate pool boiling on ribbed surfaces with micro-roughness at low moderate heat flux, ASME J. Heat Transfer 121 (1999) 376–385.